Time Evolution of Bath Properties in Spin-Boson Dynamics

Sohang Kundu[1] and Nancy Makri[1,2,*]

[1]*Department of Chemistry, University of Illinois, Urbana, Illinois 61801*
[2]*Department of Physics, University of Illinois, Urbana, Illinois 61801*
**Corresponding Author. Email: nmakri@illinois.edu*

Abstract

The dynamical behaviors of a two-level system (TLS) coupled to a harmonic dissipative bath has been studied extensively using a variety of analytical and numerical methods. The focus of the vast majority of these studies has been on the properties of the TLS, averaged with respect to the bath degrees of freedom. In this work we use real-time path integral methods to probe the behavior of select bath degrees of freedom during the dynamics of a symmetric two-level system (TLS) coupled to a dissipative bath by calculating system-bath densities (SBD) and coordinate expectation values. Overall, the SBD motion on each diabatic state is simpler than the motion of the total density. In the weak coupling regime, which characterizes the parameters of oscillators that comprise such a bath, the SBD on each TLS state remains primarily compact and Gaussian-like, such that its peak is well characterized by the mode expectation value. In the absence of a dissipative environment, nonadiabatic density depletion leads to spikes in coordinate expectation values. The evolution of the SBD peak trajectory for two discrete modes exhibits Lissajous patterns with frequency-dependent shapes which strongly resemble classical trajectory motion on a torus. These patterns become more complex when the coupling of the mode to the TLS is increased outside of this regime, leading to persistent small amplitude oscillations in the TLS populations characterized by very slow decay and SBD trajectories that exhibit behaviors reminiscent of chaotic classical systems. Indirect coupling to a dissipative bath has a stabilizing effect on the dynamics, eliminating spikes, synchronizing the SBD motion on the two diabatic states and regularizing the SBD trajectory to simple rectangular Lissajous-like shapes, regardless of the mode frequencies.

I. Introduction

The growing interest in engineering nanoscale devices with targeted function, along with the development of powerful experimental techniques for probing dynamical processes in materials and biological systems, have spurred intense interest in the direction of advancing the capabilities of quantum mechanical simulation methods. Many such methods have focused on the system-bath Hamiltonian, which continues to serve as the paradigm of dissipative phenomena[1] that generally suppress the quantum coherence of a small system.[2] Apart from its use for quantifying the parameter dependence of generic phenomena such as tunneling[3] and barrier crossing,[4] the system-bath form underlies the basic description of chemical reactions according to the reaction path Hamiltonian[5] and allows a realistic description of charge, proton and exciton transfer in a variety of situations.[6] In many such systems the bath consists of the normal mode vibrations of a molecular system or crystalline solid, while in other cases harmonic modes arise from the mapping of an anharmonic environment (e.g. solvent or protein) which is enabled by Gaussian response.

Wavefunction-based calculations of system-bath dynamics need to treat the bath explicitly and thus become costly when the number of bath degrees of freedom is large. In addition to the need for explicit treatment of harmonic bath modes, the calculation of finite temperature properties by wavefunction methods requires averaging many microcanonical results, which is impractical when the bath includes a large number of low-frequency modes. An alternative is offered by thermo-field dynamics,[7] which maps the finite-temperature density matrix on a wavefunction in an augmented space of entangled subsystems. The resulting increase of dimensionality, along with the replacement of the Boltzmann factor by its oscillatory real-time analogue, seem to offset most of the advantages gained by the absence of the thermal sum. Nevertheless, some recent work[8,9] has reported successful algorithms based on this approach.

Feynman's path integral formulation of quantum dynamics[10] offers an attractive starting point for probing the dynamics of system-bath Hamiltonians. The obvious appeal of the path integral is the ability to obtain observables pertaining to the system of interest by directly evaluating its reduced density matrix (RDM) through the sum of amplitudes, which do not require the calculation of wavefunctions.[11] An additional advantage in the case of system-bath dynamics is the ability to integrate out harmonic bath degrees of freedom analytically, replacing them by an influence functional.[12] However, evaluation of the real-time path integral requires summing astronomical number of terms, and Monte Carlo-based sampling methods fail to converge in the majority of situations because of the highly oscillatory nature of the quantum mechanical amplitude. The development of the quasi-adiabatic propagator path integral (QuAPI) methodology[13-17] during the 1990s enabled numerically exact calculations in a variety of situations. The QuAPI methodology has been employed in the study of a wide range of processes, and a number of further developments and extensions[18-29] have significantly increased the applicability of the algorithm to more demanding regimes. Further, the quantum-classical path integral,[30] a rigorous and consistent approach for integrating quantum mechanics with classical trajectory simulations, becomes numerically exact for system-bath dynamics and offers accelerated convergence in demanding regimes.[31]

The QuAPI algorithm circumvents numerical instabilities associated with phase cancellation by employing compact grid representations, and replaces the full path sum (which requires effort that increases exponentially with propagation time) by an iterative procedure which is based on the finite span of influence functional correlations. This span defines the memory length induced by the bath, which becomes a

convergence parameter. The algorithm propagates in time an array of discrete paths that span the memory length through multiplication by a propagator that includes the influence functional couplings. For a system of n states and a memory length equal to L time steps, this array is equivalent to a tensor of n^{2L} elements. For many processes of interest, this storage requirement is well within the capabilities of common computing resources.[32] Further, the vast majority of paths make negligible contributions, and a number of powerful techniques, including path filtering,[18,33] coarse graining,[25] blip[34,35] and SVD-based decompositions[28] have been employed to reduce the storage size of the sparse QuAPI tensor, offering dramatic savings in some regimes. Nevertheless, storage requirements restrict the practicality of the QuAPI methodology to small systems.

An efficient methodology is available for model baths described by the Drude spectral density form (the damped oscillator model), which involves solving hierarchical equations of motion[36] (HEOM). The method has been extended to situations where the bath spectral density is a sum of Drude terms,[37] but the cost increases steeply with the number of such terms. While not suitable for simulations of systems interacting with structured environments, the HEOM method is widely used for characterizing parameter regimes in Drude-type models of chemical processes through low-cost calculations.

A recent development showed that the tensor storage of the QuAPI algorithm can be completely eliminated. This is possible through the small matrix decomposition of the path integral[38-40] (SMatPI), where all dynamical information is contained in small $n^2 \times n^2$ matrices. Even though the path integral variables are fully entangled within the memory length, the SMatPI decomposition recursively shifts the entanglement to longer time intervals while reducing the magnitude of the entangled contributions, until they become negligible. Thus the SMatPI algorithm offers a numerically exact approach to system-bath dynamics that is free of large array storage requirements, thus is applicable to multistate systems and longer memory processes.

The vast majority of calculations involving system-bath Hamiltonians have focused on properties of the system, such as populations and expectation values (which can be obtained from the RDM) or time correlation functions. While usually the system constitutes the "observable" degree of freedom, bath modes (e.g. molecular normal modes) play a prominent role in many processes and are frequently used as a probe for understanding the mechanistic details of complex molecular processes. The charge or excitation energy transfer processes in molecular frameworks bear rich examples of this, where molecular vibrations actively participate in modulating dynamical timescales, leaving behind valuable signatures in spectroscopic measurements.

In this paper we use real-time path integral calculations to interrogate dynamical properties of the bath itself. Specifically, we focus on a symmetric two-level system (TLS) and choose one or two discrete bath modes embedded in a continuous spectral density representing a dissipative bath, and investigate their dynamics. We choose two sets of coupling parameters for these modes: In the first "weak coupling" or "spin-boson" case the mode couplings are characteristics of the values they would have if the continuous bath were discretized into an adequate number of harmonic degrees of freedom. In the second case of "moderate coupling" the coupling coefficients are representative of many vibrational modes in molecular chromophores. In each of these regimes we augment the TLS RDM with the coordinates of these modes and study the evolution of system-bath densities and coordinate expectation values. We also examine the dissipative effects of the bath on such dynamical properties. In the weak coupling case and for the parameters we study, we find that coordinate expectation values describe the motion of the density peak almost quantitatively, and that this motion can be surprisingly simple.

Even with model bath spectral densities, the parameter space that dictates the dynamics of the TLS-bath Hamiltonian is quite large, and we do not attempt to tackle a systematic study in this paper. Instead, our goal is to present some dynamical patterns that are representative of behaviors in some parameter regimes of interest.

In section II we describe the Hamiltonian that describes our model and define the basic dynamical properties that we follow. In the same section we motivate our choice of parameters, describe the basic physics of the Hamiltonian, and give a short summary of the methods that we employ to calculate the dynamics. The results of our calculations are presented in sections III and IV for the weak and moderate coupling regimes. In section V we summarize our findings and present some concluding remarks.

II. Spin-boson models, observables and methods

Our model consists of a two-level system (TLS) coupled to one or two discrete harmonic oscillator modes, with coordinates q_1, q_2, frequencies ω_1, ω_2 and coupling coefficients c_1, c_2, as well as a dissipative harmonic bath. The Hamiltonian is

$$\hat{H} = -\hbar\Omega\left(\left|\mathrm{R}\right\rangle\left\langle\mathrm{L}\right| + \left|\mathrm{L}\right\rangle\left\langle\mathrm{R}\right|\right) + \sum_{i=1}^{2}\left(\frac{\hat{p}_i^2}{2m} + \frac{1}{2}m\omega_i^2\left(\hat{q}_i - \frac{c_i\hat{s}}{m\omega_i^2}\right)^2\right) + \sum_{i=1}^{\infty}\left(\frac{\hat{p}_{\mathrm{b},i}}{2m} + \frac{1}{2}m\omega_{\mathrm{b},i}^2\left(\hat{q}_{\mathrm{b},i} - \frac{c_{\mathrm{b},i}\hat{s}}{m\omega_{\mathrm{b},i}^2}\right)^2\right) \quad (2.1)$$

where the two system states are denoted as R and L, $\hat{s} = s_{\mathrm{R}}\left|\mathrm{R}\right\rangle\left\langle\mathrm{R}\right| + s_{\mathrm{L}}\left|\mathrm{L}\right\rangle\left\langle\mathrm{L}\right|$ is the operator (with eigenvalues $s_{\mathrm{R}}, s_{\mathrm{L}}$) that specifies the system state, the parameters of the discrete modes are ω_1, c_1 and ω_2, c_2, and the tunneling splitting of the isolated TLS is $2\hbar\Omega$. By setting $c_2 = 0$ we study the dynamics with a single discrete mode. The TLS states often represent electronic states which may characterize charge or exciton transfer processes. The discrete modes may represent intramolecular normal mode vibrations, while the bath, which is often used to represent a solvent or biological environment, describes a large number of additional degrees of freedom (with a practically continuous frequency distribution) which couple to the TLS and introduce dissipative interactions.

A bath described by a continuous spectral density is equivalent to an infinite number of harmonic oscillators whose frequencies and coupling parameters of the dissipative bath are characterized by the spectral density function[3]

$$J(\omega) = \frac{1}{2}\pi\sum_i \frac{c_{\mathrm{b},i}^2}{m_i\omega_{\mathrm{b},i}}\delta\left(\omega - \omega_{\mathrm{b},i}\right). \quad (2.2)$$

In many situations it is convenient to discretize the bath into n harmonic modes. The number n of oscillators is arbitrary, constrained only by the requirement that the dynamics of the original and discretized baths must match up to the desired propagation time. This sets a lower bound on the value of n for a particular propagation length. In typical situations, propagation over short to intermediate times requires 50-200 discretized modes, while larger values are needed for longer propagation. Based on earlier theoretical considerations and scaling ideas,[41] the coupling coefficients scales as $1/\sqrt{n}$, and efficient discretization algorithms are available.[42,43]

With these ideas in mind, we consider the choice of coupling constants for the "weak coupling" or "spin-boson" regime. Our goal is to investigate the dynamical properties of modes that comprise the dissipative bath under consideration. For the frequency of interest, we consider a sufficiently large value of the discretization parameter n and choose c_i by requiring[43] that the reorganization energy λ_i of the mode equals $1/n$ of the total bath reorganization energy λ. We note that different properties have different convergence characteristics with the number of discretization modes. Once n is sufficiently large we observe some simple patterns that do not change upon further increasing this parameter.

To investigate the "moderate coupling" or "molecular vibration" regime, we consider larger values of c_i which are vaguely consistent with the Huang-Rhys factors[44] of common intramolecular vibrations. Such coupling parameters are known to vary over several orders of magnitude,[45] and we consider values that characterize vibrations that couple to the electronic states with small to moderate strength. In this paper we do not consider strongly coupled modes. Strong coupling leads to vibronic dynamics that can lead to behaviors that are entirely different from those that we describe in this work. Such effects are investigated in another paper. In all cases the coupling coefficients are chosen to satisfy the relation $c_i = \kappa\omega_i$ where the proportionality factor κ has the same value for the two discrete modes, ensuring that they make equal contributions to the reorganization energy.

In most of the calculations presented in sections IV and V we use the standard Ohmic spectral density function, $J(\omega) = \frac{1}{2}\pi\hbar\xi\omega e^{-\omega/\omega_c}$, to describe the dissipative bath. This form leads to rich dynamical behaviors[3] and has been used in countless theoretical studies. However, one might wonder whether the generic behavior we identify are intimately connected to the broad, unstructured Ohmic function. To clarify this concern, we also present some results using a structured spectral density obtained by rescaling a function obtained from molecular dynamics simulations of a biological process, rescaled to a frequency range and reorganization energy similar to those in our model calculations. We find that the behaviors we observe remain qualitatively unchanged as long as the spectral density corresponds to dissipative dynamics, regardless of its detailed appearance.

Each of the two TLS states, along with the discrete and the bath modes, defines a diabatic potential energy surface. The two surfaces are displaced with respect to the $q_i = 0$ axes by the amounts $q_i^{\min} = \pm c_i/m\omega_i^2$. With the chosen parameters this displacement is small compared to the span of eigenfunctions and the zero-point energy of each diabatic potential lies above the curve crossing point. Figure 1 shows the diabatic and adiabatic potential curves for the TLS coupled to the first discrete mode. Also shown are the squares (the densities) of the diabatic wavefunctions, i.e. the projections of the eigenfunctions on the R and L TLS states. It is seen that the ground state density peaks on the inner side of the diabatic potential minima, i.e. $\left|q_i^{\text{peak}}\right| < \left|q_i^{\min}\right|$. This effective anharmonicity, which arises arising from coupling to the TLS, leads to shifts in the average value of oscillatory observables presented later.

At $t = 0$ the TLS is assumed to be in the R state, while the two modes as well as the continuous bath are described by Boltzmann distributions centered about the coordinates $q_i = 0$ and $q_{\text{b},i} = 0$. These initial conditions characterize the density matrix generated by a "vertical" Franck-Condon transition from the ground electronic state of a molecular system.

In common system-bath calculations, observables are defined with the respect to the TLS alone and the reduced density matrix (RDM) is calculated. In this work we probe the dynamics of the TLS and the discrete modes in the presence of the dissipative bath. In our recent investigations of excitation energy transfer dynamics in the dimer of a perylene bisimide we defined the one- and two-mode electronic-vibrational densities[46] by partially summing the full density matrix, which was expressed in terms of the

intramolecular normal mode coordinates of each molecule. These quantities allowed us to explore the nonadiabatic dynamics in that system at a high level of detail and to elucidate the origins of various features of the excitation transfer process that stem from the interplay between electronic and vibrational motion. Here we define analogous one- and two-mode system-bath densities (SBD) for each TLS state,

$$\begin{aligned} D_1^{\mathrm{R}}(q_1,t) &= \mathrm{Tr}_{\mathrm{b}} \left\langle \mathrm{R}q_1 \left| e^{-i\hat{H}t/\hbar} \hat{\rho}(0) e^{i\hat{H}t/\hbar} \right| \mathrm{R}q_1 \right\rangle \\ D_{12}^{\mathrm{R}}(q_1,q_2,t) &= \mathrm{Tr}_{\mathrm{b}} \left\langle \mathrm{R}q_1q_2 \left| e^{-i\hat{H}t/\hbar} \hat{\rho}(0) e^{i\hat{H}t/\hbar} \right| \mathrm{R}q_1q_2 \right\rangle \end{aligned} \tag{2.3}$$

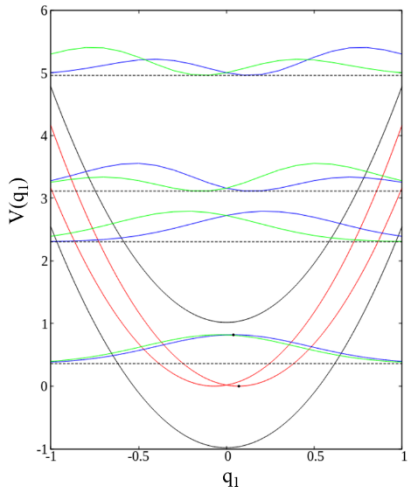

Fig. 1. Diabatic (red) and adiabatic (black) potential energy functions for a discrete mode with $\omega_1 = 2.7$, $c_1 = 0.5$ and $\Omega = 1$. Blue and green lines show the squares of the four lowest eigenfunctions projected on the R and L states, respectively. The dashed lines indicate the eigenvalues. The two dots mark the R diabatic potential minimum and the corresponding density maximum.

From these SBD functions we obtain expectation values of the discrete mode coordinates on each state,

$$\left\langle q_i^{\mathrm{R}}(t) \right\rangle = \frac{\int dq_i \; q_i D_1^{\mathrm{R}}(q_i,t)}{\int dq_i \; D_1^{\mathrm{R}}(q_i,t)} \quad \text{or} \quad \left\langle q_i^{\mathrm{R}}(t) \right\rangle = \frac{\int dq_1 \int dq_2 \; q_i D_{12}^{\mathrm{R}}(q_1,q_2,t)}{\int dq_1 \int dq_2 \; D_{12}^{\mathrm{R}}(q_1,q_2,t)}, \; i = 1,2\,, \tag{2.4}$$

as appropriate. The normalization coefficients in the denominators are the R- and L-state populations that are needed to account for the variation in probability density due to population transfer between the two system states. We also define the total SBD

$$\begin{aligned} D_1(q_1,t) &= D_1^{\mathrm{R}}(q_1,t) + D_1^{\mathrm{L}}(q_1,t) \\ D_{12}(q_1,q_2,t) &= D_{12}^{\mathrm{R}}(q_1,q_2,t) + D_{12}^{\mathrm{L}}(q_1,q_2,t) \end{aligned} \tag{2.5}$$

and the corresponding mode coordinate expectation values

$$\left\langle q_i\,(t)\right\rangle = \int dq_i\ q_i D_1\left(q_i,t\right) \quad \text{and} \quad \left\langle q_i\,(t)\right\rangle = \int dq_1 \int dq_2\, q_i D_{12}\left(q_1,q_2,t\right),\ i=1,2\,. \tag{2.6}$$

Calculations for one or two discrete modes coupled to the TLS were performed with a standard basis set code which uses a direct product of TLS and harmonic oscillator basis functions. The procedure was described in detail in another paper.[47]

All results involving a dissipative bath were obtained using the SMatPI methodology.[38-40] Given an initial condition, the RDM is obtained from the matrix product

$$\tilde{\rho}_{i_N^{\pm}}\left(N\Delta t\right) = \sum_{i_0^{\pm}=1}^{n} U^{(N0)}_{i_N^{\pm} i_0^{\pm}} \tilde{\rho}_{i_0^{\pm}}\left(0\right) \tag{2.7}$$

where $i_k^{\pm} = \mathrm{R,L}$ is the index that specifies the state of the TLS, $\Delta t = t/N$ is the path integral time step and

$$U^{(N0)}_{i_N^{\pm} i_0^{\pm}} = \mathrm{Tr}_{\mathrm{b}} \left\langle s_{i_N^{+}} \left| e^{-i\hat{H}N\Delta t/\hbar} \right| s_{i_0^{+}} \right\rangle \hat{\rho}_{\mathrm{vib}}(0) \left\langle s_{i_0^{-}} \left| e^{i\hat{H}N\Delta t/\hbar} \right| s_{i_N^{-}} \right\rangle \tag{2.8}$$

is the reduced propagator, which is averaged with respect to the bath. Its path integral expression is given by the sum

$$U^{(N0)}_{i_N^{\pm} i_0^{\pm}} = \sum_{i_{N-1}^{\pm}=1}^{n} \cdots \sum_{i_1^{\pm}=1}^{n} G_{i_N^{\pm}, i_{N-1}^{\pm}} \cdots G_{i_1^{\pm}, i_0^{\pm}} F_{i_N^{\pm}, i_{N-1}^{\pm}, \ldots, i_0^{\pm}} \tag{2.9}$$

where $G_{i_k^{\pm}, i_{k-1}^{\pm}}$ are short-time forward-backward propagators for the system Hamiltonian and $F_{i_N^{\pm}, i_{N-1}^{\pm}, \ldots, i_0^{\pm}}$ is the QuAPI-discretized influence functional,[48,49] which contains memory terms that couple the path integral variables. If the memory spans L path integral time steps, evaluation of the RDM can be performed through the QuAPI algorithm,[15,16] which involves iteration in time and leads to linear scaling with the number of time steps. In the case of a system characterized by *n* states, the QuAPI algorithm[15,16] generally requires the storage of a tensor of n^{2L} path amplitudes and involves n^{2L+2} operations for each propagation step. In many situations, the number of paths that must be stored can be dramatically reduced through filtering criteria[18,33,50] or singular value decomposition.[27] Further, under certain conditions characteristic of incoherent dynamics, the blip decomposition[35,51] reduces the array storage to just the blip configurations. Nevertheless, the storage requirements of these algorithms can be impractical for treating systems with multiple states.

The SMatPI algorithm[38-40] is a decomposition of the path integral expression (2.9) that eliminates the tensor storage requirements of the iterative QuAPI algorithm. The SMatPI decomposition disentangles the path integral variables, leading to an algorithm that involves only the storage of small matrices. Propagation of the reduced propagator beyond the memory length is given by the form

$$\mathbf{U}^{(N0)} = \sum_{r=1}^{N-1} \mathbf{M}^{(N,N-r)} \cdot \mathbf{U}^{(N-r,0)} + \mathbf{M}^{(N0)}, \quad N = 2,\ldots \tag{2.10}$$

where $\mathbf{M}^{(Nm)}$ are $n^2 \times n^2$ matrices that are recursively obtained from the full path integral expression with the discretized influence functional. The main cost of the algorithm is in the generation of these matrices, i.e. the cost of the entire calculation is comparable to that of a single QuAPI iteration. Most importantly, the elimination of large tensor storage allows the inclusion of much longer memory, as well as the treatment of multistate systems.

III. Spin-boson regime: Dynamics of weakly coupled modes

In this and the next section we set $\Omega = 1$. With this value the tunneling splitting of the bare TLS is equal to 2 energy units. We choose the frequencies $\omega_1 = 2.7$ and $\omega_2 = 3.2$ for the discrete modes. The dissipative bath has an Ohmic spectral density with a cutoff frequency $\omega_c = 7.5$.

First, we present results with a single discrete mode of $\omega_1 = 2.7$ weakly coupled to the TLS with $c_1 = 0.1$, at two temperatures that correspond to $\beta = 5$ and 0.05. Figure 2 shows nine representative frames (chosen as those that best capture the important dynamical features) of the SBD time evolution on the R and L states for the two chosen temperatures. At the lower of these temperatures the initial density is that of a Gaussian with width approximately equal to that of the harmonic oscillator ground state. The small displacement of the SBD leads to motion reminiscent of Gaussian wavepacket dynamics, i.e. the density remains compact and Gaussian-like on each of the two diabatic curves, although nonadiabatic effects lead to density transfer between the two states. The effects of this motion on the TLS population dynamics, shown in Figure 3, are almost imperceptible. However, we emphasize that the collective effect of many bath modes in this frequency and coupling range can be very significant.

Several states of the special mode are populated at the higher temperature, resulting in a much broader SBD and introducing contributions from multiple eigenvalues. The combination with nonadiabatic effects leads to less trivial SBD evolution, where two and even three small humps are observed in some low-density frames. The population exhibits quantum beat patterns in this case.

Figures 4 and 5 show the normalized position expectation values of the discrete mode $\langle q_1^{\mathrm{R}}(t) \rangle$ and $\langle q_1^{\mathrm{L}}(t) \rangle$ on each of the two TLS states, and also $\langle q_1(t) \rangle$ with respect to the total density, as a function of time for the TLS coupled to only this mode and also in the presence of the dissipative bath. For comparison, the coordinate expectation value is also shown for the dissipationless mode in the absence of electronic coupling. In the $\Omega = 0$ case the density remains Gaussian at all times and its peak coincides with the averaged coordinate, thus $\langle q_1^{\mathrm{R}}(t) \rangle$ oscillates between the inner and outer turning points, which on the R state are located at $q_1^{\mathrm{in}} = 0$ and $q_1^{\mathrm{out}} = 2q_1^{\mathrm{min}}$, respectively.

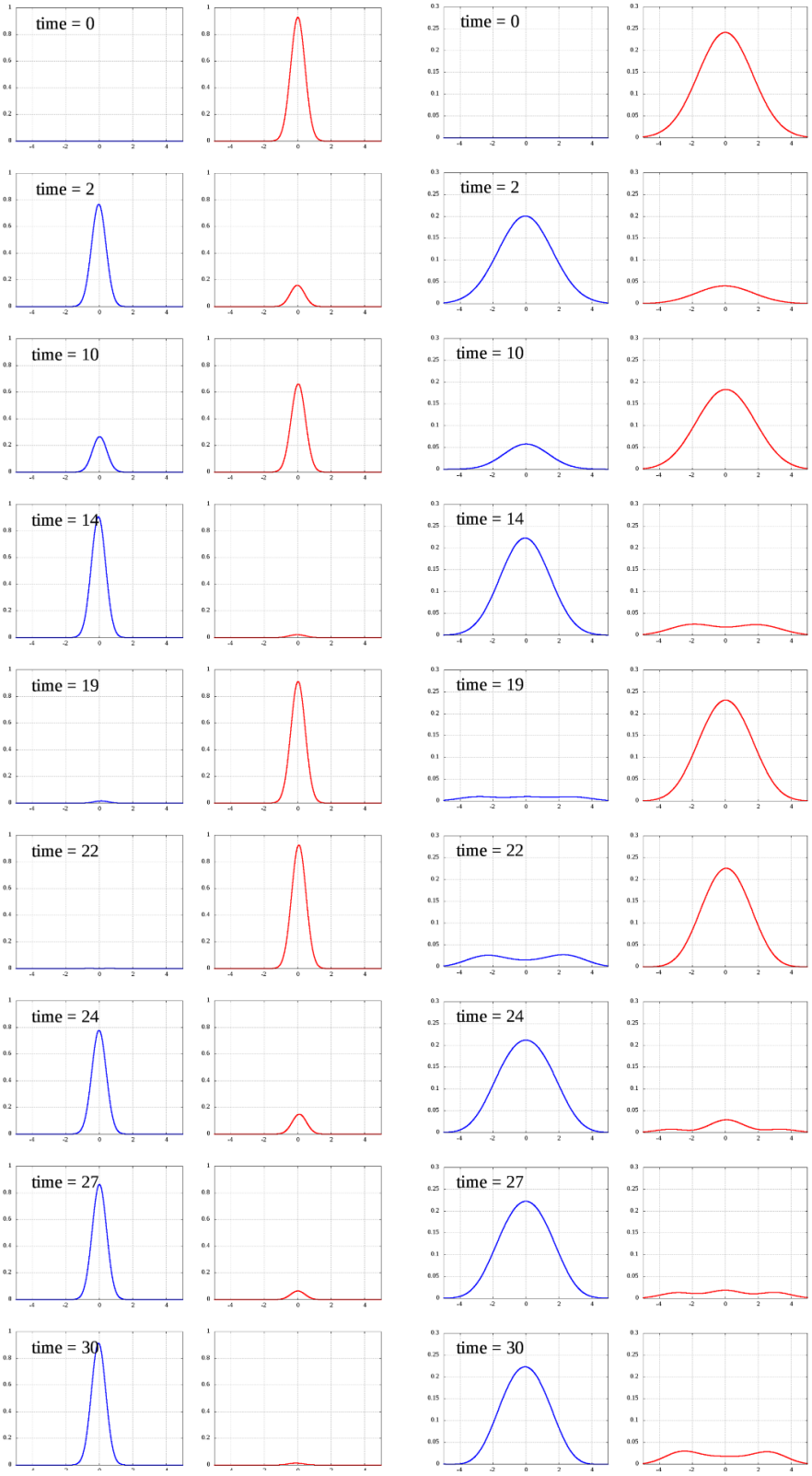

Fig. 2. Time evolution of SBD on the two states for $\omega_1 = 2.7$ and $c_1 = 0.1$. At each time, the density on the R (red) and L (blue) state is shown as a function of the mode coordinate q_1 (horizontal axis). Left: $\beta = 5$. Right: $\beta = 0.05$.

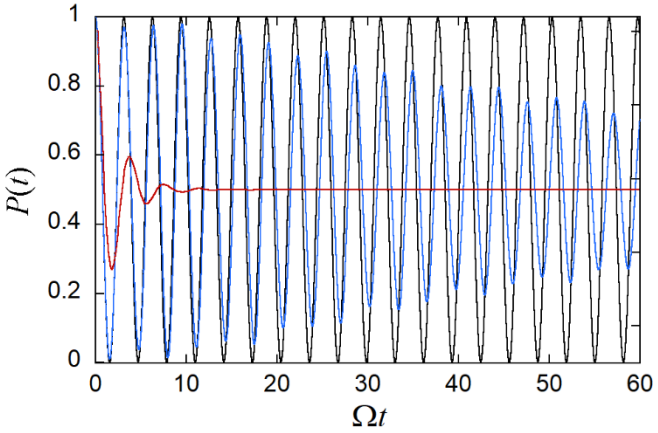

Fig. 3. Population of R state as a function of time for the weakly coupled mode with $\omega_1 = 2.7$ and $c_1 = 0.1$. Black and blue lines: $\xi = 0$ at two temperatures, $\beta = 5$ and $\beta = 0.05$. Red line: $\xi = 0.2$, $\beta = 5$.

Nonadiabatic effects lead to major changes in the evolution of mode observables. When the continuous bath is present, the averaged mode coordinate exhibits simple oscillatory patterns. However, the oscillation amplitude on each state is increased significantly relative to the $J = 0$, while the mean value of $\langle q_1^{\mathrm{R}}(t) \rangle$ is decreased. The inward shift of the average mode coordinates is a consequence of anharmonicity, which results in skewed wavefunctions as shown in Fig. 1. The increased oscillation amplitude is a consequence of SBD depletion and is discussed below. Further, it is worth noting that the oscillations of the coordinate expectations values (thus the peak densities) on the R and L states are synchronized. The coordinate expectation value with respect to the total density (right panel of Figure 4) also displays similar oscillations, although more variability appears at early times.

In the absence of the bath the evolution of the averaged mode coordinate on each TLS state exhibits spikes that occur at periodic intervals. The pattern around these spikes alternates between two behaviors, namely spikes where the averaged mode coordinate on the R state exhibits large positive values on both sides of the spike, and those where the large values have opposite signs on the two sides of the spike. It is seen that the spikes are less prominent at high temperature. In that case the overall appearance of the mode expectation value is smoother.

The average mode coordinate with respect to the total density does not display spikes, as the total density does not get depleted, but the oscillation pattern is not as simple as that observed on each of the two diabatic states. When two discrete modes are considered, the behavior of the expectation value with respect to the total density becomes even more complex, while simple, physically meaningful patterns are observed when the coordinates are averaged with respect to the individual state densities. For this reason we focus on the single-state expectation values, $\langle q_1^{\mathrm{R}}(t) \rangle$ and $\langle q_1^{\mathrm{L}}(t) \rangle$.

We now turn to an explanation for the spikes in the coordinate expectation values. As seen in Fig. 4, the average mode coordinate (and the SBD peak position) on each TLS state extends far beyond the outer turning point in the case of $\Omega > 0$. When the population is transferred between the R and L states, SBD depletion in the region surrounding the crossing point ($q_1 = 0$) pushes the SBD maximum to very large

values. In the absence of a bath, the population evolution shown in Fig. 3 shows that depletion is quantitative at certain times, leading to spikes in the average mode coordinate. This effect is amplified when the mode coupling is small, implying that the SBD range on each state and the nonadiabatic region where state crossing is likely[52] overlap significantly. As back-transfer takes place, adding SBD density to the R state from the opposite side (i.e. from density on the L state, whose maximum lies to the left of the curve crossing point), the mode expectation value spikes with the opposite sign. The opposite effect is observed in the next half cycle of the electronic dynamics, i.e. during the first recurrence of R population. We note again that the oscillation of the mode average coordinate is not symmetric with respect to the diabatic potential minimum. This effect, which is a consequence of diabatic coupling-induced anharmonicity, is seen more clearly in the case where the TLS is coupled to a dissipative bath, for which the oscillation pattern is simpler. As the temperature is increased, asynchronous contributions from higher excited states prevent a significant depletion of the SBD, gradually washing out the spikes. However, we emphasize that the density is not compact and Gaussian-like at this high temperature, so the coordinate expectation value does not have the same simple physical interpretation of peak position in this case.

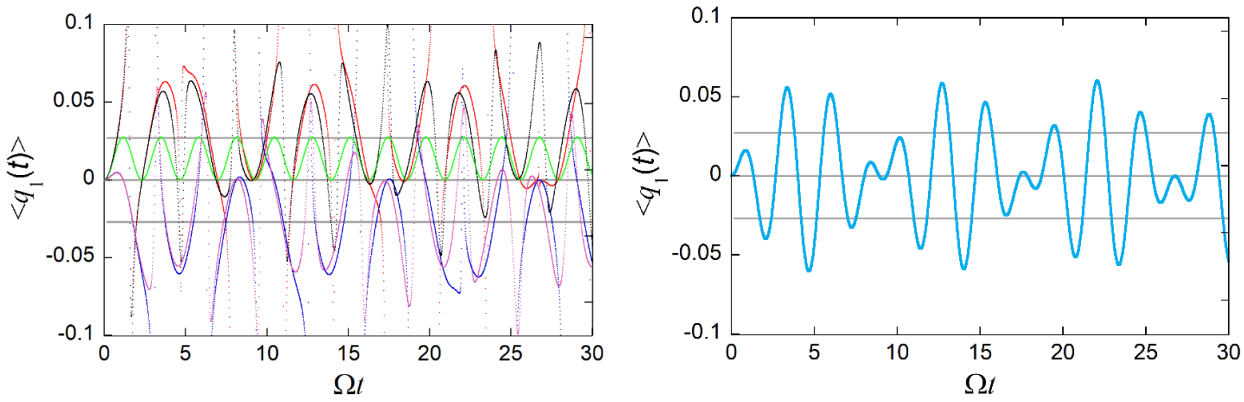

Fig. 4. Coordinate expectation value for the discrete mode with $\omega_1 = 2.7$ and $c_1 = 0.1$ at two temperatures. The horizontal lines indicate the turning points on the diabatic potentials. Left: expectation values on each of the two states. Red and blue: $\langle q_1^{\mathrm{R}}(t)\rangle$ and $\langle q_1^{\mathrm{L}}(t)\rangle$, $\beta = 5$. Black and magenta: $\langle q_1^{\mathrm{R}}(t)\rangle$ and $\langle q_1^{\mathrm{L}}(t)\rangle$, $\beta = 0.05$. The green line shows the coordinate expectation value for $\Omega = 0$. Right: coordinate expectation value $\langle q_1(t)\rangle$ with respect to the total density, when $\beta = 0.05$.

In the presence of a dissipative bath, the apparent constant-amplitude oscillation of the coordinate expectation value do not persist indefinitely. This behavior is a consequence of the dissipative nature of the dynamics, although the indirect interaction (through the TLS) of the mode with the bath leads to very slow decay. Figure 5 shows the time evolution of $\langle q_1^{\mathrm{R}}(t)\rangle$ for the lower temperature over a long time interval. This very slow decay of oscillation amplitude is the result of energy exchange between the discrete mode and the bath, which is mediated by the TLS, as the harmonic modes are not coupled directly in the Hamiltonian. The dissipative effects of the continuous bath lead both the TLS populations and observables associated with the discrete mode to equilibrium, albeit equilibration of these properties occurs on very different time scales.

Next, we present results for a TLS coupled to both discrete modes. Just as observed in the single-mode calculations, the density on each state remains compact and Gaussian-like with these parameters, such that the coordinates obtained from the position expectation values practically coincide with the location of the SBD peak.

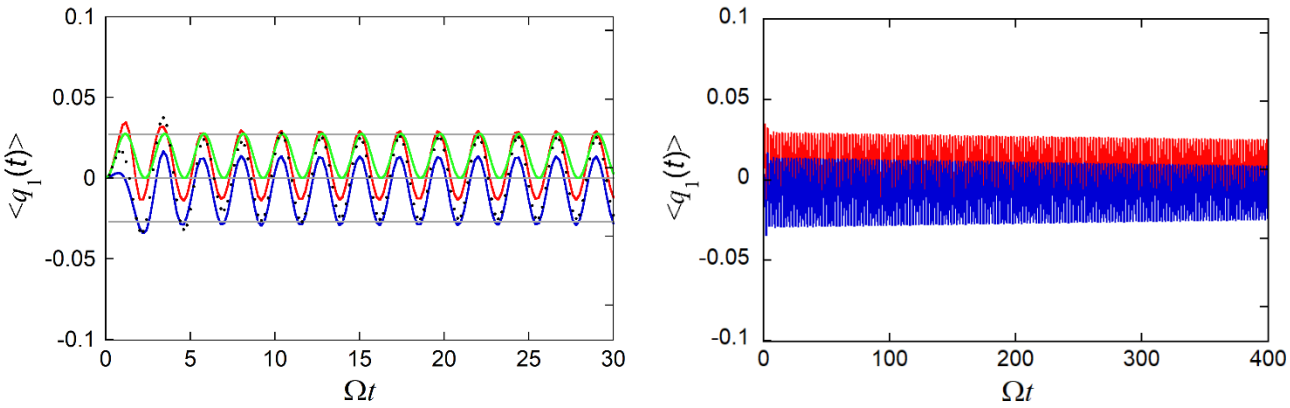

Fig. 5. Coordinate expectation values for the discrete mode with $\omega_1 = 2.7$ and $c_1 = 0.1$ at $\beta = 5$. Red and blue lines show $\langle q_1^{\mathrm{R}}(t)\rangle$ and $\langle q_1^{\mathrm{L}}(t)\rangle$, respectively, and the black markers show $\langle q_1(t)\rangle$. The green line shows the coordinate expectation value for $\Omega = 0$. The horizontal lines indicate the turning points on the diabatic potentials. The evolution of the expectation values $\langle q_1^{\mathrm{R}}(t)\rangle$ and $\langle q_1^{\mathrm{L}}(t)\rangle$ over a much longer time is shown in the right panel.

Figure 6 shows the "trajectory" of the SBD peak on the R state, i.e. $\langle q_2^{\mathrm{R}}(t)\rangle$ vs. $\langle q_1^{\mathrm{R}}(t)\rangle$, over a time period $t = 240$ (which corresponds to ~76 TLS periods) for the TLS coupled to two discrete modes with various frequency ratios, where again color indicates the density value. The spikes observed in Fig. 4, which correspond to low density regions, show as yellow-tinted loops that surround a region of Lissajous-type appearance with clear boundaries. These regular patterns resemble the behavior of classical trajectories in integrable systems, or (more generally) trajectory dynamics on KAM tori, and as is well known,[53,54] the particular shape that is observed depends on the value of the characteristic winding number of the torus (which is given by the local relation of the classical frequencies and thus depends on anharmonicity effects). At zero temperature, where the evolving density results from a single initial state, the SBD trajectory is confined within a two-dimensional region that has the topology of a square, and which is embedded within the larger energetically available region bounded by the curve $V(q_1, q_2) = E$. These patterns observed in Fig. 6 are a consequence of the compact, Gaussian-like evolution of the SBD on each diabatic state.

Shown in Figure 7 is the evolution of the SBD peak for the two discrete modes in the presence of a dissipative bath for one of the parameters of Fig. 6 over the same time length. As observed in the single-mode dynamics, even weak coupling to a dissipative bath prevents populations from falling to zero, thus eliminating spikes and outside loops, while further smoothing and regularizing the dynamics. After a short excursion that reflects early-time transient behavior, the coordinate expectation values settle into a regular classical-like pattern with a rectangular boundary. Note that the boundary of the SBD trajectory is rectangular in all cases, regardless of the complexity of the Lissajous pattern observed with different mode frequency ratios in the absence of a dissipative bath. The change of the SBD trajectory induced by the

indirect dissipative effects of the bath (which the discrete modes experience exclusively through their coupling to the TLS) is dramatic for some of the parameters, in particular when the frequencies are close to a low-order resonance condition, turning twisted, pretzel-shaped trajectories into simple patterns reminiscent of classical motion with irrational frequency relations.

In line with the shift of the oscillation region discussed in the single-mode case, both axes of the SBD rectangle are shifted. Further, the size of the rectangular region is decreased, reflecting the amplitude reduction through dissipative interactions, which lead to energy exchange between discrete mode and the bath. The amplitude rescaling due to the bath varies for different frequency modes, leading to rectangular Lissajous-like patterns of varying aspect ratios.

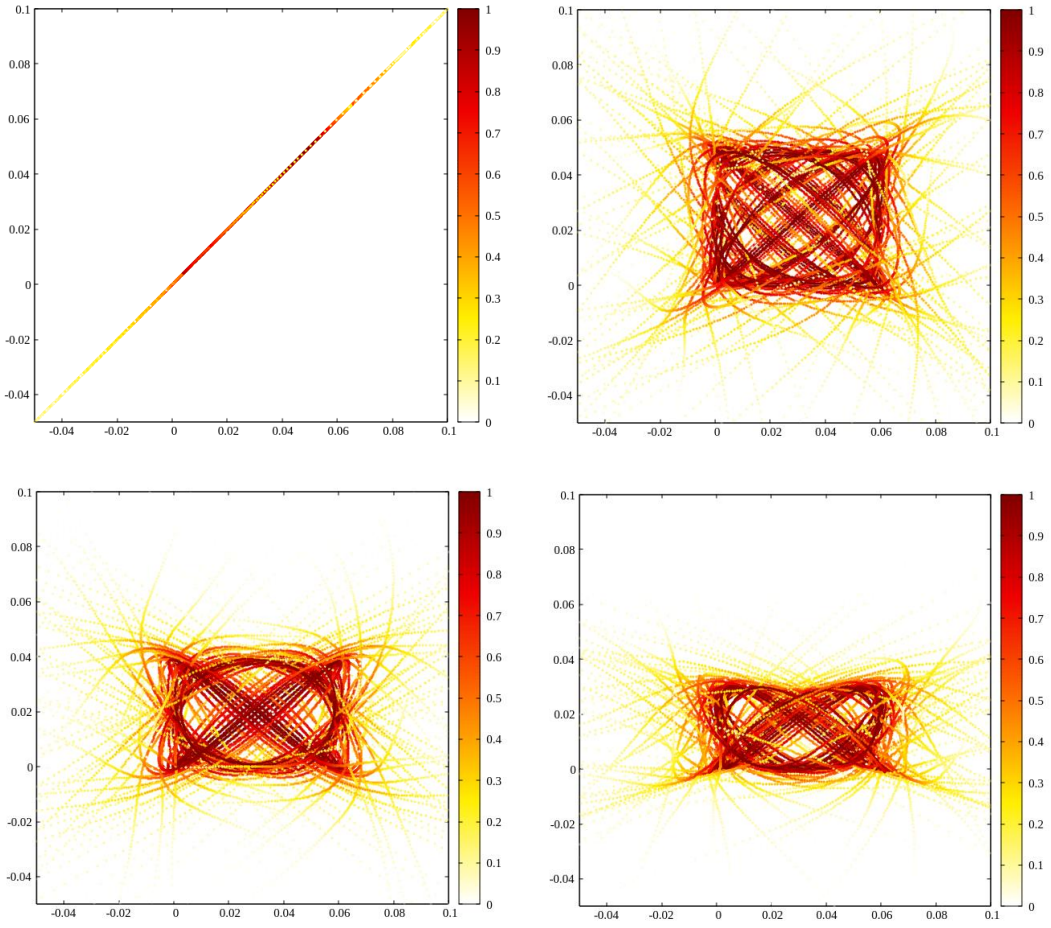

Fig. 6. Trajectory of SBD peak on the R state, i.e. coordinate expectation values $\langle q_2^{\mathrm{R}}(t)\rangle$ (vertical axis) vs. $\langle q_1^{\mathrm{R}}(t)\rangle$ (horizontal axis) for the discrete modes on the R state for $\beta = 5$ in the absence of a dissipative bath up to $t = 240$. In all cases the parameters of the first discrete mode are $\omega_1 = 2.7$, $c_1 = 0.1$. Top left: $\omega_2 = 2.7$, $c_2 = 0.1$. Top right: $\omega_2 = 2.9$, $c_2 = 0.1074$. Bottom left: $\omega_2 = 3.2$, $c_2 = 0.12$. Bottom right: $\omega_2 = 3.6$, $c_2 = 0.1333$. The color intensity (from white to yellow to red) indicates the value of the R state population.

Also shown in Fig. 7 is the SBD trajectory in the presence of the bath over a much longer time interval. The color intensity in the second panel indicates the time value. As the amplitude of the SBD motion gradually decreases, the rectangular Lissajous region shrinks. Thus the SBD trajectory displays resembles regular motion with an attractor[54] in this case. However, the dissipative effects depend on the mode frequency and the strength of indirect coupling to the bath via the TLS, thus the amplitudes of the two modes decay with different rates. For example, a mode with a larger displacement or strong effective coupling will show a faster decay of the oscillation amplitude, due to more rapid indirect energy exchange with other modes. Therefore, this effect leads to a Lissajous boundary with an evolving aspect ratio, where the long and short sides of the rectangle may eventually switch, as we see in the next section. However, we emphasize that amplitude decay in the small coupling regime is extremely slow, leading to simpler patterns, i.e. the SBD trajectory amplitude is practically constant over time intervals much longer than the characteristic time of TLS RDM dynamics.

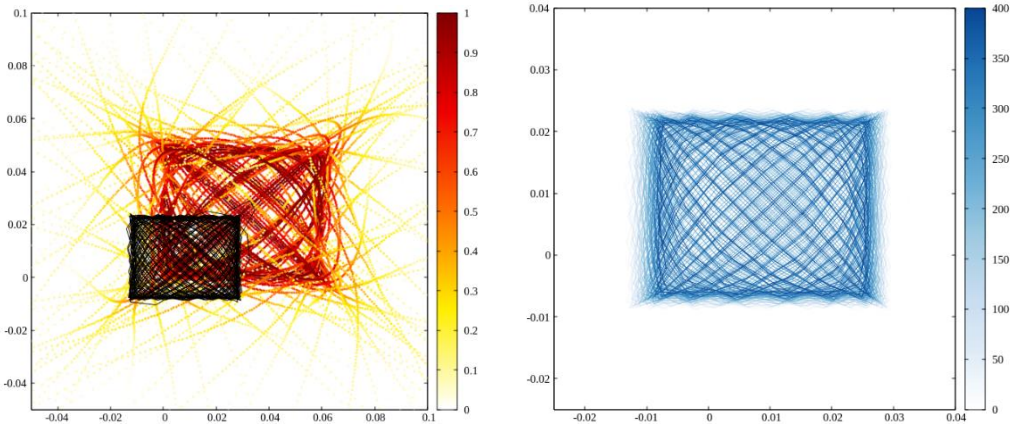

Fig. 7. Trajectory of SBD peak on the R state, i.e. coordinate expectation values $\langle q_2^{\mathrm{R}}(t)\rangle$ (vertical axis) vs. $\langle q_1^{\mathrm{R}}(t)\rangle$ (horizontal axis), for the discrete modes with $\omega_1 = 2.7$, $c_1 = 0.1$ and $\omega_2 = 2.9$, $c_2 = 0.1074$ on the R state, in the presence of a dissipative bath with $\xi = 0.1$. The left panel shows the trajectory over a time interval $t = 240$. The trajectory of the SBD peak is shown in black. No color variation is used in this case because coupling to the bath eliminates low-density regions. The SBD trajectory for $\xi = 0$ is also shown in the background for comparison. The right panel shows the SBD trajectory for a very long time, $\Omega t = 400$. The color intensity indicates the time value.

The above results indicate indirect coupling to a dissipative bath leads to profound changes in the motion of the SBD in the weak coupling regime representative of discrete bath modes characterizing a continuous spectral density. This indirect interaction leads to the smoothing of the SBD, preventing it from falling to zero and thus regularizing the peak trajectory, the synchronization of the SBD trajectory on the two diabatic states, and the destruction of twisted trajectory patterns resulting from low-order resonance relations by simpler structures reminiscent of irrational tori in classical dynamical systems. If the coupling of the probed modes is weak, the regular evolution of the SBD trajectory continues for very long times.

These behaviors pose a new question: Are the regularizing effects of the bath the result of broad spectral densities with a smooth distribution of coupling parameters? To clarify this, we replace the Ohmic spectral density by a highly structured form obtained from molecular dynamics simulations of a biological electron transfer process,[55] scaled to roughly match the reorganization energy and time scales of our models. Figure 8 shows the coordinate expectation value on the R and L states for the mode at the second major peak of the spectral density, which is indicated with an arrow. The coupling constant was obtained by discretizing the spectral density into $n \simeq 500$ modes. The mode expectation value exhibits the behaviors observed with the Ohmic spectral density: the oscillations are smooth, free of the sharp patterns observed in the absence of a dissipative bath, the mean value of the oscillations are shifted with respect to the diabatic minima (a consequence of anharmonicity induced by nonadiabatic coupling), and the oscillations on the R and L states are rapidly synchronized. These behaviors suggest that the stabilizing effects of the bath on the SBD of a weakly coupled mode are not the result of a broad spectral density in the vicinity of the mode frequency. Rather, these smoothing effects are a consequence of the overall dissipative dynamics induced by a bath characterized by a continuous spectral density, which may be broad or structured.

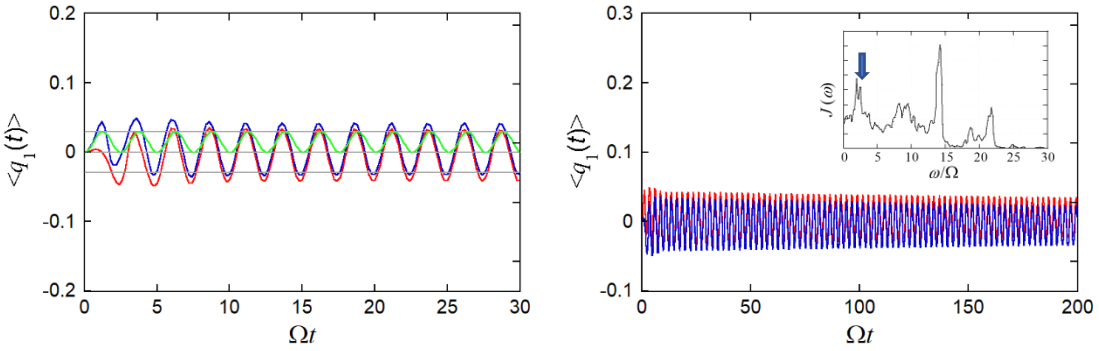

Fig. 8. Coordinate expectation values for the structured spectral density shown in the inset of the right panel. The frequency of the chosen mode is indicated with an arrow. Red and blue lines show $\langle q_1^{\mathrm{R}}(t) \rangle$ and $\langle q_1^{\mathrm{L}}(t) \rangle$. The green line shows the coordinate expectation value in the absence of nonadiabatic coupling. The horizontal lines indicate the turning points on the diabatic potentials. The evolution of the expectation values $\langle q_1^{\mathrm{R}}(t) \rangle$ and $\langle q_1^{\mathrm{L}}(t) \rangle$ over a much longer time is shown in the right panel.

IV. Molecular vibration regime: Dynamics of modes coupled to the TLS with moderate strength

Figure 9 shows the SBD time evolution on the R and L states for the same frequency used in the previous section, $\omega_1 = 2.7$, but with a larger coupling value, $c_1 = 0.5$. In the low temperature case the SBD is again seen to remain compact and Gaussian-like. However, the shape of the SBD is very significantly modified at the high temperature, where anharmonicity arising from nonadiabatic dynamics introduces pronounced oscillatory components.

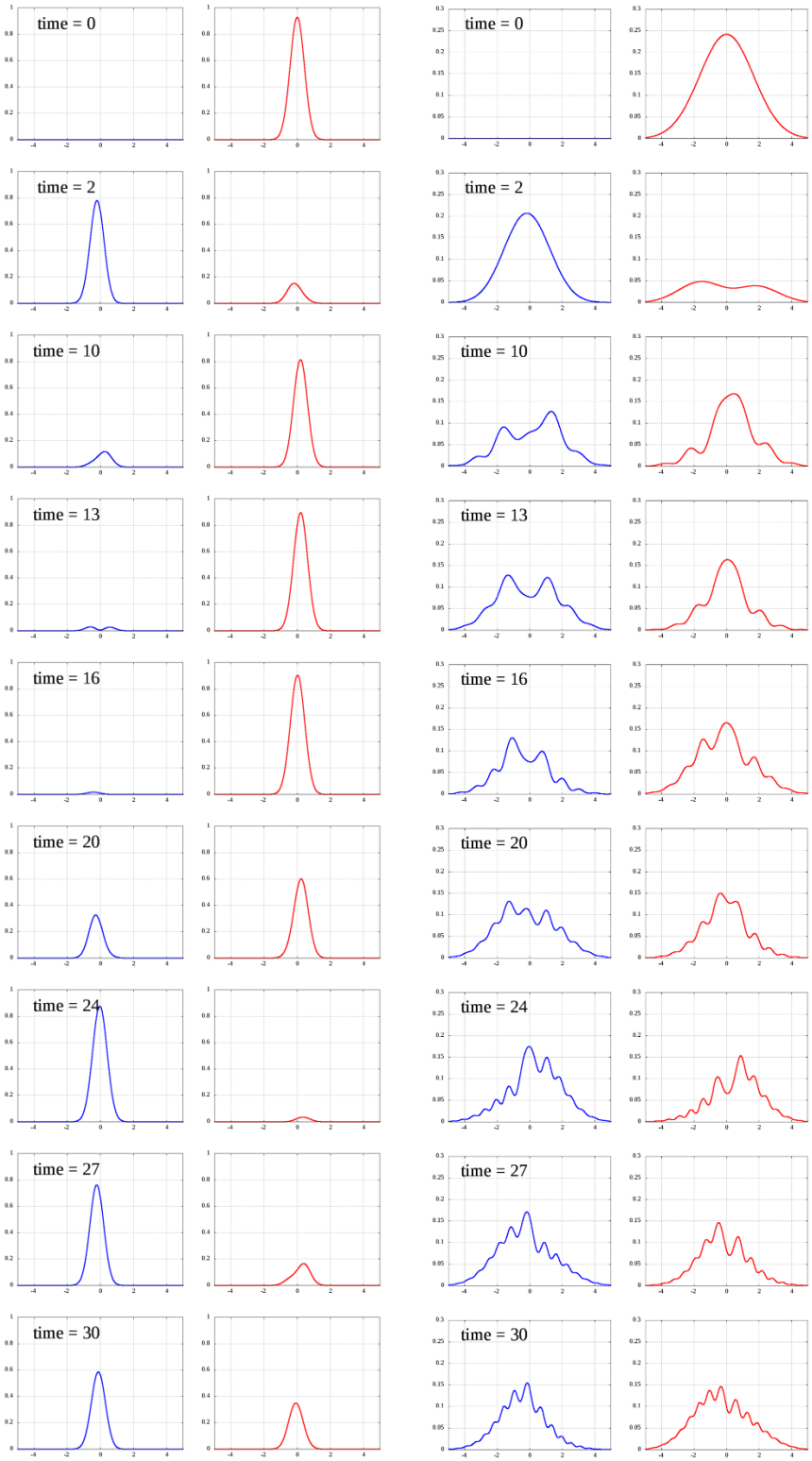

Fig. 9. Time evolution of SBD on the two states for $\omega_1 = 2.7$ and $c_1 = 0.5$. At each time, the density on the R (red) and L (blue) state is shown as a function of the mode coordinate q_1. Left: $\beta = 5$. Right: $\beta = 0.05$.

.

The time evolution of the population of the R TLS state is shown in Figure 10. With this stronger TLS-mode coupling the population exhibits quantum beat patterns which survive even in the presence of a dissipative bath. In sharp contrast to the common situation of a TLS coupled only to a dissipative environment, the TLS population in the present case displays persistent oscillations which do not die out within the typical time scale associated with RDM dynamics. The magnitude of these oscillations is moderate at the low temperature and small but not negligible at the high temperature.

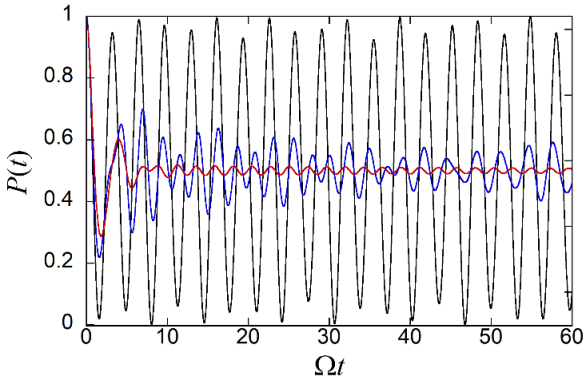

Fig. 10. Population of R state as a function of time for the weakly coupled mode with $\omega_1 = 2.7$ and $c_1 = 0.5$. Black and blue lines: $\xi = 0$, $\beta = 5$ and $\beta = 0.05$. Red line: $\xi = 0.2$, $\beta = 5$.

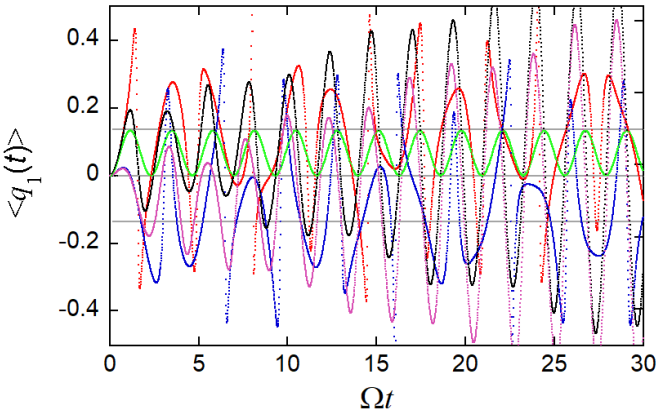

Fig. 11. Coordinate expectation value for the discrete mode on the two states with $\omega_1 = 2.7$ and $c_1 = 0.5$ for two temperatures. Red and blue: $\langle q_1^{R}(t)\rangle$ and $\langle q_1^{L}(t)\rangle$, $\beta = 5$. Black and magenta: $\langle q_1^{R}(t)\rangle$ and $\langle q_1^{L}(t)\rangle$, $\beta = 0.05$. The green line shows the coordinate expectation value for $\Omega = 0$. The horizontal lines indicate the turning points on the diabatic potentials.

Figures 11 and 12 show the normalized position expectation values of the discrete mode, $\langle q_1^{\mathrm{R}}(t)\rangle$ and $\langle q_1^{\mathrm{L}}(t)\rangle$, on each of the two TLS states as a function of time for the TLS coupled to only this mode and also in the presence of a dissipative bath with $\xi = 0.2$, $\omega_c = 7.5$ and $\beta = 5$. These figures the analogues of figures 4 and 5 for stronger coupling. The dynamical patterns in these figures are qualitatively similar to those observed in the case of a weakly coupled mode. However, the spikes in the average mode coordinate are not as prominent in the present case, reflecting the absence of very low SBD regions. In turn, the latter is a consequence of density retention on the diabatic surfaces which was identified in our recent study[56] of nonadiabatic dynamics in the PBI dimer in strong system-bath coupling regimes. Again, the oscillations of the coordinate expectation values on the R and L states are perfectly synchronized.

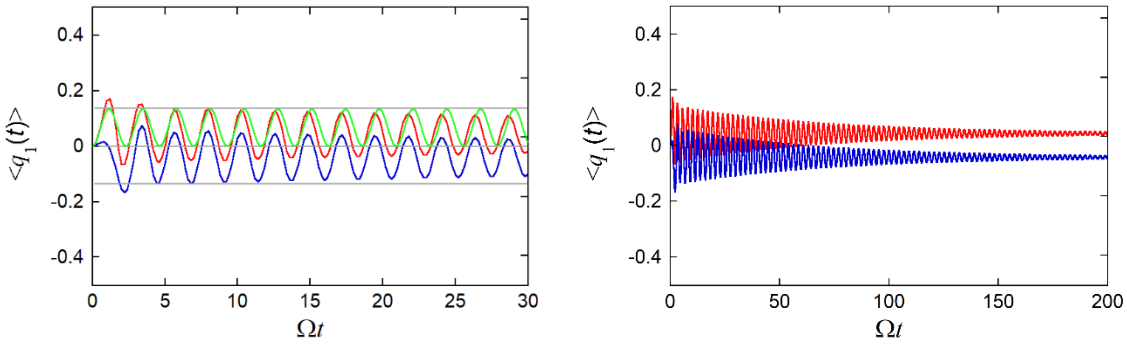

Fig. 12. Coordinate expectation value on the two states for the discrete mode with $\omega_1 = 2.7$ and $c_1 = 0.5$ at $\beta = 5$. Red and blue lines show $\langle q_1^{\mathrm{R}}(t)\rangle$ and $\langle q_1^{\mathrm{L}}(t)\rangle$, respectively. The green line shows the coordinate expectation value for $\Omega = 0$. The horizontal lines indicate the turning points on the diabatic potentials. The evolution of the expectation values $\langle q_1^{\mathrm{R}}(t)\rangle$ and $\langle q_1^{\mathrm{L}}(t)\rangle$ over a much longer time is shown in the right panel.

In the presence of a dissipative bath, Fig. 12 shows a noticeable difference in the motion of the SBD compared to the weak coupling case. The decay of the oscillation amplitude is now noticeable even within the short time interval shown in the left panel of Fig. 12. This accelerated decay is the result of faster energy transfer to the bath, facilitated by the larger coupling strength to the TLS.

Last, in Figures 13 and 14 we show the SBD trajectory in the presence of the bath for two modes (with the frequency combinations used in section III) for moderately large coupling parameters. These two figures are the moderate coupling counterparts of Figures 6 and 7. In the absence of coupling to the dissipative bath, the SBD trajectories exhibit very different dynamics. The regular Lissajous-type patterns observed in the weak coupling case (Fig. 7) are strongly perturbed and the distinct shapes are now hardly recognizable. Fig. 13 shows that under strong coupling the SBD trajectories resemble unwound balls of yarn with no clear trajectory boundaries. The observed patterns are reminiscent of chaotic motion in classical systems, where trajectories are not confined on tori and can thus explore higher dimensional regions.

In spite of the loss of regular trajectory dynamics with increased mode-TLS coupling strength, interaction with a dissipative bath again simplifies the motion. The resulting SBD trajectory shows again the simple rectangular Lissajous pattern observed in the weak coupling case. As the two mode oscillation amplitudes decay faster in this case and with different rates, the long-time evolution of the SBD trajectory displays a substantial change, where the rectangular region shrinks and eventually changes aspect ratio.

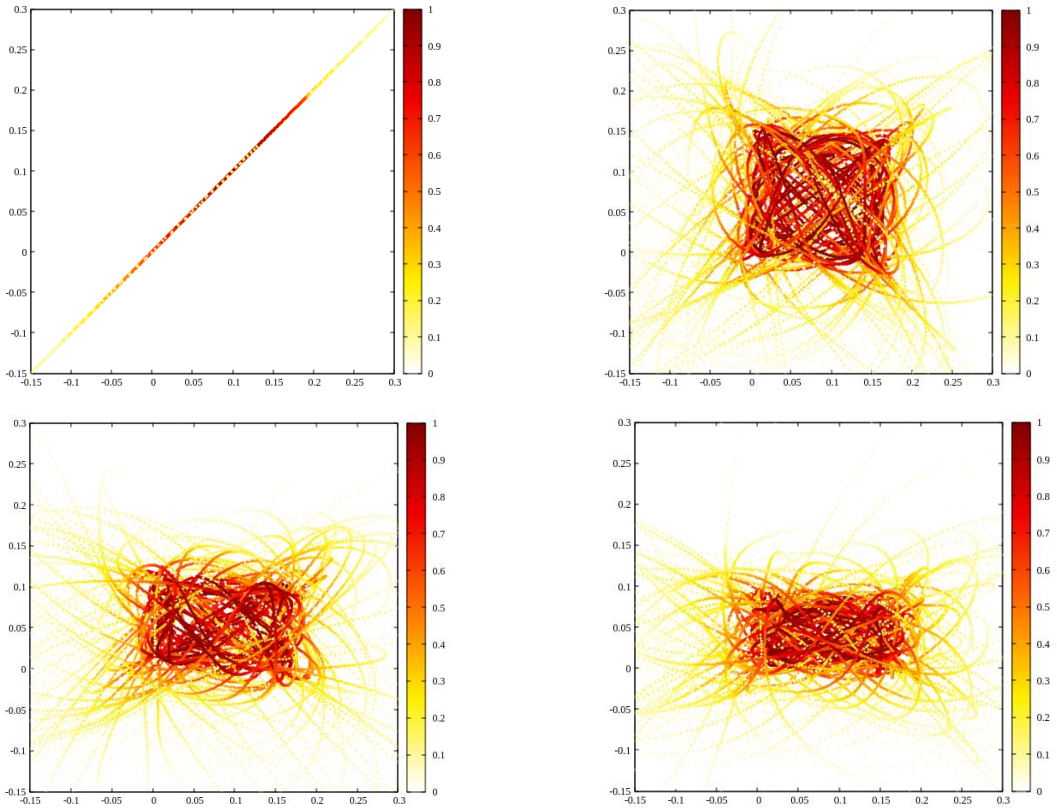

Fig. 13. Trajectory of SBD peak on the R state, i.e. coordinate expectation values $\langle q_2^{\mathrm{R}}(t)\rangle$ (vertical axis) vs. $\langle q_1^{\mathrm{R}}(t)\rangle$ (horizontal axis), for the discrete modes on the R state for $\beta = 5$ in the absence of a dissipative bath up to $\Omega t = 240$. In all cases the parameters of the first discrete mode are $\omega_1 = 2.7$, $c_1 = 0.3$. Top left: $\omega_2 = 2.7$, $c_2 = 0.3$. Top right: $\omega_2 = 2.9$, $c_2 = 0.32$. Bottom left: $\omega_2 = 3.2$, $c_2 = 0.35$. Bottom right: $\omega_2 = 3.6$, $c_1 = 0.4$. The color intensity (from white to yellow to red) indicates the value of the R state population.

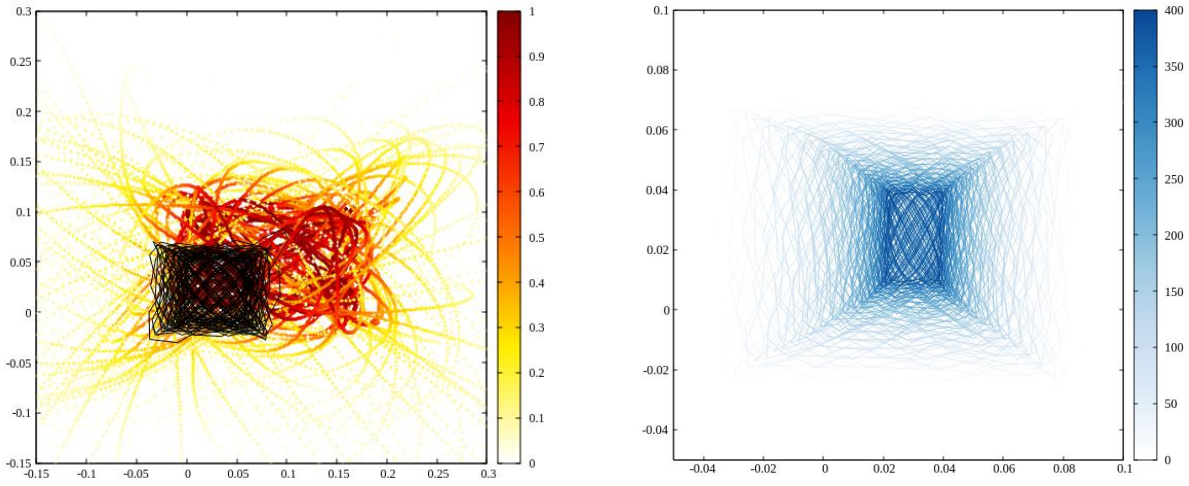

Fig. 14. Trajectory of SBD peak on the R state, i.e. coordinate expectation values $\left\langle q_2^{\mathrm{R}}(t)\right\rangle$ (vertical axis) vs. $\left\langle q_1^{\mathrm{R}}(t)\right\rangle$ (horizontal axis), for two discrete modes with $\omega_1 = 2.7$, $c_1 = 0.3$ and $\omega_1 = 3.2$, $c_1 = 0.35$ on the R state. The colored line shows results in the absence of a bath. The left panel shows the trajectory over a time interval $t = 240$. The color variation (from yellow to red) indicates the value of the R state population. The black line shows the trajectory of the SBD peak for $\xi = 0.2$. The right panel shows the SBD trajectory for the same bath parameters for a very long time ($t = 400$). The color intensity indicates the time value. Note the change in aspect ratio of the rectangular region (landscape at early times, portrait at long times).

V. Concluding Remarks

In this paper we have explored dynamical behaviors in dissipative two-level systems from the perspective of the bath. Rather than focusing on properties pertaining to the TLS, such as populations and coherences, which are encoded in the RDM, we investigated the dynamics of the bath itself. Specifically, we calculated the time evolution of the SBD functions, i.e. the densities on the two TLS states along the coordinates of one or two discrete modes of the bath, and the expectation values of these coordinates over very long times in two coupling regimes.

The first regime characterizes the parameters of bath modes obtained from a very fine discretization of a continuous spectral density. We argued that one can always choose a sufficiently large number of discrete modes that reproduce the dynamics of any observable over a chosen time length. Since the coupling coefficients become smaller as the number of modes increases, each mode of a discretized bath is characterized by small coupling, and we refer to this situation as the weak coupling or spin-boson regime. We studied the dynamics of one and two such modes with frequencies larger than the TLS tunneling parameter.

In this weak coupling regime, our calculations showed that at low temperatures the nonadiabatic dynamics of one or two discrete modes coupled to a TLS is characterized by a Gaussian-like density which is almost entirely depleted during the state-to-state transfer. The near-Gaussian shape of the density implies that its peak is well characterized by the coordinate expectation value, which we calculate. As the density is nearly depleted, its remaining small peak appears to travel far beyond the energetically allowed region, leading to spikes in the coordinate expectation value. Aside from these spikes, the SBD trajectory exhibits Lissajous patterns strongly reminiscent of regular classical dynamics, whose specifics reflect the frequency relation on the particular torus. More complex dynamical effects are observed at high temperatures, where the density is broadened and no longer Gaussian-like.

The indirect coupling of the chosen discrete modes to a dissipative bath leads to very important changes in the dynamics. The SBD becomes even smoother and its complete depletion is prevented, leading to the elimination of spikes in coordinate expectation values. The trajectory of the SBD peak is smoothed, and the motion on the R and L states is rapidly synchronized. The changes induced through indirect coupling to a dissipative bath are even more pronounced in the trajectories of two discrete modes. Our calculations showed that the complex, frequency-specific patterns observed in the absence of the dissipative bath are entirely eliminated, giving rise to simpler generic Lissajous oscillations within rectangular regions. The boundaries of these regions shrink over very long time periods, reflecting the slow decrease in oscillation amplitudes. As noted above, the mode coupling parameters can be made arbitrarily small by increasing the number of discrete bath oscillators, thus the boundaries of the SBD trajectories can remain stable over extremely long times. By using a structured spectral density of a shape that was parameterized for a biological electron transfer reaction, we show that these behaviors are not specific to smooth spectral densities characteristic of simple models and are not contingent upon the existence of a broad background around the frequency of the chosen mode.

The moderate coupling regime corresponds to coupling coefficients that are considerably larger than those in the spin-boson regime. Such parameters are often encountered in molecular vibrations coupled to two electronic states and are measured through Huang-Rhys factors. Under low-temperature conditions we observed some significant changes in the dynamics of SBD evolution and coordinate expectation values. Even though the SBD remains primarily compact and Gaussian-like on each surface, the noticeable density retention during transfer prevents the SBD peak from traveling far beyond the expected region marked by the turning points of the harmonic oscillator, leading to smoother expectation values. However, the regular Lissajous patterns in the two-mode SBD trajectories are severely perturbed and no longer resemble trajectory motion on a torus. Interestingly, coupling to a dissipative bath restores the regular character of the SBD dynamics in this regime as well.

In this study we did not attempt to present a systematic exploration of the TLS-bath parameter space. We chose frequencies larger than the TLS tunneling parameter, for which the resulting dynamics was somewhat simple, yet very interesting behaviors of bath dynamics emerged from our calculations. Further, we did not consider strongly coupled modes. Our recent work on excitation energy transfer in molecular aggregates of bacteriochlorophyll and dyes revealed a host of interesting effects in moderate-to-strong coupling regimes, which are characterized by significant complexity. Thus, the combination of studies based on simple models and molecular Hamiltonians yields complementary perspectives and rich information.

Acknowledgments

This material is based upon work supported by the National Science Foundation under Award CHE-1955302**.** This research is part of the Blue Waters sustained-petascale computing project, which is supported by the National Science Foundation (Awards OCI-0725070 and ACI-1238993) and the state of Illinois. Blue Waters is a joint effort of the University of Illinois at Urbana-Champaign and its National Center for Supercomputing Applications.

References

1. Caldeira, A. O.; Leggett, A. J., Path integral approach to quantum Brownian motion. *Physica A* **1983**, 121, 587-616.
2. Weiss, U., *Quantum Dissipative Systems*. World Scientific: Singapore, 1993.
3. Leggett, A. J.; Chakravarty, S.; Dorsey, A. T.; Fisher, M. P. A.; Garg, A.; Zwerger, M., Dynamics of the dissipative two-state system. *Rev. Mod. Phys.* **1987**, 59, 1-85.
4. Kramers, H. A., Brownian motion an a field of force and the diffusion model of chemical reactions. *Physica (Utrecht)* **1940**, 7, 284-304.
5. Miller, W. H.; Handy, N. C.; Adams, J. E., Reaction path Hamiltonian for polyatomic molecules. *J. Chem. Phys.* **1980**, 72, 99-112.
6. May, V.; Kühn, O., *Charge and energy transfer dynamics in molecular systems*. 3rd ed.; Wiley: 2011.
7. Takahashi, Y.; Umezawa, H. T. f. d., Thermo field dynamics. *int. J. Mod. Phys. B* **1996**, 19, 1755-1805.
8. Borrelli, R.; Gelin, M. F., Quantum electron-vibrational dynamics at finite temperature: Thermo field dynamics approach. *The Journal of Chemical Physics* **2016**, 145, 224101.
9. Chen, L.; Zhao, Y., Finite temperature dynamics of a Holstein polaron: The thermo-field dynamics approach. *The Journal of Chemical Physics* **2017**, 147, 214102.
10. Feynman, R. P., Space-time approach to non-relativistic quantum mechanics. *Rev. Mod. Phys.* **1948**, 20, 367-387.
11. Feynman, R. P.; Hibbs, A. R., *Quantum Mechanics and Path Integrals*. McGraw-Hill: New York, 1965.
12. Feynman, R. P.; F. L. Vernon, J., The theory of a general quantum system interacting with a linear dissipative system. *Ann. Phys.* **1963**, 24, 118-173.
13. Makri, N., Improved Feynman propagators on a grid and non-adiabatic corrections within the path integral framework. *Chem. Phys. Lett.* **1992**, 193, 435-444.
14. Topaler, M.; Makri, N., System-specific discrete variable representations for path integral calculations with quasi-adiabatic propagators. *Chem. Phys. Lett.* **1993**, 210, 448.
15. Makri, N.; Makarov, D. E., Tensor multiplication for iterative quantum time evolution of reduced density matrices. I. Theory. *J. Chem. Phys.* **1995**, 102, 4600-4610.
16. Makri, N.; Makarov, D. E., Tensor multiplication for iterative quantum time evolution of reduced density matrices. II. Numerical methodology. *J. Chem. Phys.* **1995**, 102, 4611-4618.
17. Sim, E.; Makri, N., Filtered propagator functional for iterative dynamics of quantum dissipative systems. *Comp. Phys. Commun.* **1997**, 99, 335-354.
18. Sim, E., Quantum dynamics for a system coupled to slow baths: on-the-fly filtered propagator method. *J. Chem. Phys.* **2001**, 115, 4450-4456.
19. Shao, J.; Makri, N., Iterative path integral calculation of quantum correlation functions for dissipative systems. *Chem. Phys.* **2001**, 268, 1-10.
20. Shao, J.; Makri, N., Iterative path integral formulation of equilibrium correlation functions for quantum dissipative systems. *J. Chem. Phys.* **2002**, 116, 507-514.
21. Weiss, S.; Eckel, J.; Thorwart, M.; Egger, R., Iterative real-time path integral approach to nonequilibrium quantum transport. *Phys. Rev. B* **2008**, 77, 195316.

22. Segal, D.; Millis, A. J.; Reichman, D. R., Numerically exact path integral simulation of nonequilibrium quantum transport and dissipation. *Phys. Rev. B* **2010**, 82, 205323.
23. Simine, L.; Segal, D., Path integral simulations with fermionic and bosonic reservoirs: Transport and dissipation in molecular electronic junctions. *J. Chem. Phys.* **2013**, 138, 214111.
24. Makri, N., Path integral renormalization for quantum dissipative dynamics with multiple timescales. *Mol. Phys.* **2012**, 110, 1001-1007.
25. Richter, M.; Fingerhut, B. P., Coarse-grained representation of the quasiadiabatic propagator path integral for the treatment of non-Markovian long-time bath memory. *J. Chem. Phys.* **2017**, 146, 214101.
26. Palm, P.; Nalbach, P., Quasi-adiabatic path integral approach for quantum systems under the influence of multiple non-commuting fluctuations. *J. Chem. Phys.* **2018**, 149, 214103
27. Straatsma, T. P.; Lovett, B. W.; Kirton, P., Efficient real-time path integrals for non-Markovian spin-boson models. *New Journal of Physics* **2017**, 19, 093009.
28. Strathearn, A.; Kirton, P.; Kilda, D.; Keeling, J.; Lovett, B. W., Efficient non-Markovian quantum dynamics using time-evolving matrix product operators. *Nature Communications* **2018**, 9, 3322.
29. Sato, Y., A scalable algorithm of numerical real-time path integral for quantum dissipative systems. *J. Chem. Phys.* **2019**, 150, 224108.
30. Lambert, R.; Makri, N., Quantum-classical path integral: Numerical formulation. *J. Chem. Phys.* **2012**, 137, 22A553.
31. Makri, N., Quantum-classical path integral: A rigorous approach to condensed phase dynamics. *International Journal of Quantum Chemistry* **2015**, 115, 1209-1214.
32. Makri, N., Quantum dissipative systems: a numerically exact methodology. *J. Phys. Chem.* **1998**, 102, 4414-4427.
33. Sim, E.; Makri, N., Tensor propagator with weight-selected paths for quantum dissipative dynamics with long-memory kernels. *Chem. Phys. Lett.* **1996**, 249, 224-230.
34. Makri, N., Exploiting classical decoherence in dissipative quantum dynamics: Memory, phonon emission, and the blip sum. *Chem. Phys. Lett.* **2014**, 593, 93-103.
35. Makri, N., Iterative blip-summed path integral for quantum dynamics in strongly dissipative environments. *J. Chem. Phys.* **2017**, 146, 134101.
36. Ishizaki, A.; Tanimura, Y., Quantum Dynamics of System Strongly Coupled to Low-Temperature Colored Noise Bath: Reduced Hierarchy Equations Approach. *Journal of the Physics Society Japan* **2005**, 74, 3131-3134.
37. Liu, H.; Zhu, L.; Bai, S.; Shi, Q., Reduced quantum dynamics with arbitrary bath spectral densities: Hierarchical equations of motion based on several different bath decomposition schemes. *The Journal of Chemical Physics* **2014**, 140, 134106.
38. Makri, N., Small matrix disentanglement of the path integral: overcoming the exponential tensor scaling with memory length. *J. Chem. Phys.* **2020**, 152, 041104.
39. Makri, N., Small matrix path integral for system-bath dynamics. *Journal of Chemical Theory and Computation* **2020**, 16, 4038–4049.
40. Makri, N., Small matrix path integral with extended memory. *J. Chem. Theory and Comput.* **2021**, 17, 1-6.
41. Suarez, A.; Silbey, R., Properties of a macroscopic system as a thermal bath. *J. Chem. Phys.* **1991**, 95, 9115-9121.

42. Makri, N., The linear response approximation and its lowest order corrections: an influence functional approach. *J. Phys. Chem.* **1999**, 103, 2823-2829.
43. Walters, P. L.; Allen, T. C.; Makri, N., Direct determination of harmonic bath parameters from molecular dynamics simulations. *J. Comput. Chem.* **2017**, 38, 110-115.
44. Huang, K.; Rhys, A., Theory of light absorption and non-radiative transitions in F-centres. *Proceedings of the Royal Society of London. Series A. Mathematical and Physical Sciences* **1950**, 204.
45. Schröter, M.; Ivanov, S. D.; Schulze, J.; Polyutov, S. P.; Yan, Y.; Pullerits, T.; Kühn, O., Exciton–vibrational coupling in the dynamics and spectroscopy of Frenkel excitons in molecular aggregates. *Physics Reports* **2015**, 567, 1-78.
46. Kundu, S.; Makri, N., Origin of vibrational features in the excitation energy transfer dynamics of perylene bisimide J-aggregates. *J. Chem. Phys.* **2021**, 114301.
47. Kundu, S.; Makri, N., Exciton-vibration dynamics in J-aggregates of a perylene bisimide from real-time path integral calculations. *J. Phys. Chem. C* **2021**, 125, 201-210.
48. Makri, N., Numerical path integral techniques for long-time quantum dynamics of dissipative systems. *J. Math. Phys.* **1995**, 36, 2430-2456.
49. Allen, T. C.; Walters, P. L.; Makri, N., Direct computation of influence functional coefficients from numerical correlation functions. *J. Chem. Theory and Comput.* **2016**, 12, 4169-4177.
50. Lambert, R.; Makri, N., Memory path propagator matrix for long-time dissipative charge transport dynamics. *Mol. Phys.* **2012**, 110, 1967-1975.
51. Makri, N., Blip decomposition of the path integral: Exponential acceleration of real-time calculations for quantum dissipative systems. *J. Chem. Phys.* **2014**, 141, 134117.
52. Wolynes, P. G., Dissipation, tunneling and adiabaticity criteria for curve crossing problems in the condensed phase. *J. Chem. Phys.* **1987**, 86, 1957-1966.
53. Gutzwiller, M. C., *Chaos in classical and quantum mechanics*. Springer: New York, 1990.
54. Lichtenberg, A.; Lieberman, M., *Regular and chaotic dynamics*. 2nd ed.; Springer: 1992.
55. Marchi, M.; Gehlen, J. N.; Chandler, D.; Newton, M., Diabatic surfaces and the pathway for primary electron transfer in a photosynthetic reaction center. *J. Am. Chem. Soc.* **1993**, 115, 4178-4190.
56. Kundu, S.; Makri, N., Electronic-vibrational density evolution in a perylene bisimide dimer: mechanistic insights into excitation energy transfer. *Phys. Chem. Chem. Phys.* **2021**, in press.